

Structure of a Na^+/H^+ antiporter and insights into mechanism of action and regulation by pH

Carola Hunte¹, Emanuela Screpanti¹, Miro Venturi¹, Abraham Rimon², Etana Padan² & Hartmut Michel¹

The control by Na^+/H^+ antiporters of sodium/proton concentration and cell volume is crucial for the viability of all cells. Adaptation to high salinity and/or extreme pH in plants and bacteria or in human heart muscles requires the action of Na^+/H^+ antiporters. Their activity is tightly controlled by pH. Here we present the crystal structure of pH-downregulated NhaA, the main antiporter of *Escherichia coli* and many enterobacteria. A negatively charged ion funnel opens to the cytoplasm and ends in the middle of the membrane at the putative ion-binding site. There, a unique assembly of two pairs of short helices connected by crossed, extended chains creates a balanced electrostatic environment. We propose that the binding of charged substrates causes an electric imbalance, inducing movements, that permit a rapid alternating-access mechanism. This ion-exchange machinery is regulated by a conformational change elicited by a pH signal perceived at the entry to the cytoplasmic funnel.

Regulation of intracellular pH, cellular Na^+ content and cell volume are processes that are essential for all living cells. Na^+/H^+ antiporters¹ have primary functions in these crucial processes^{2–4}. They are integral membrane proteins that are ubiquitous throughout all biological kingdoms; a change in their activity can have an immediate impact on cell metabolism and viability. For example, overactivation of the NHE1 antiporter in heart muscle cells during open-heart surgery in humans has harmful consequences, which are reduced by the use of drugs inhibiting the antiporter^{5,6}. Deletion of plant genes encoding the vacuolar and cytoplasmic membrane Na^+/H^+ antiporters decreases the plant's salt tolerance^{7,8}, whereas overexpressing is exploited to produce salt-resistant plants⁹. Although belonging to different protein families², many prokaryotic Na^+/H^+ antiporters confer on their host cells Na^+ tolerance and/or a capacity to grow at alkaline pH (refs 2, 10). Na^+/H^+ antiporters have also been implicated in the virulence and/or epidemiology of pathogenic enterobacteria¹¹.

NhaA is the main Na^+/H^+ antiporter of *Escherichia coli* and many other enterobacteria¹². Its orthologues are widespread in many other prokaryotes including Archaea. NhaA uses the electrochemical proton gradient maintained across the bacterial membrane and excretes Na^+ in exchange for a 'downhill' flow of protons into the cell¹². NhaA activity is strictly regulated by pH, a property it shares with many other prokaryotic^{12,13} and eukaryotic^{14,15} antiporters and which is essential for cytoplasmic pH regulation. At acidic pH NhaA is downregulated^{12,16}, a feature that permits the formation of crystals ordered well enough to determine its architecture and to reveal the structural basis for a mechanism of Na^+/H^+ exchange and its unique regulation by pH. The structure of NhaA represents a previously undescribed fold that contributes to the understanding of the architecture of membrane proteins in general.

Structure determination

X-ray diffraction data were collected from native and seleno-L-methionine (SeMet)-labelled crystals grown at pH 4.0. Statistics for

data collection and structure determination are summarized in Supplementary Table S1. NhaA crystallized in space group $P2_12_12_1$ with two monomers in the asymmetric unit present in an opposite, non-physiological orientation (Fig. 1a). In the native membrane¹⁷ and in two-dimensional crystals^{18,19}, NhaA is known to form a dimer.

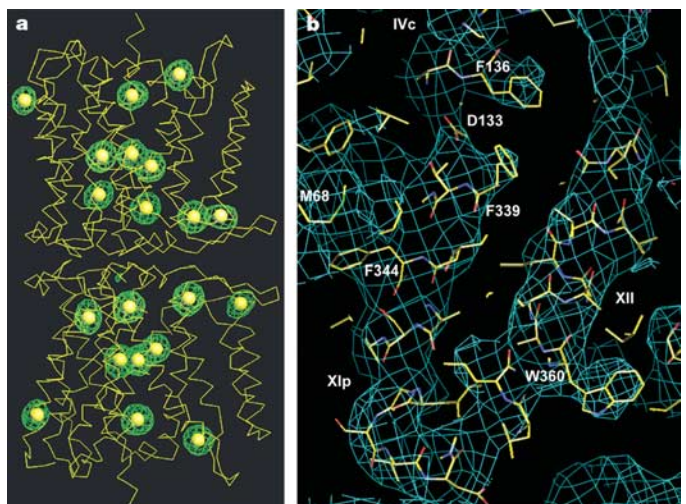


Figure 1 | Experimental electron density. **a**, Side view of the backbone of two NhaA molecules related by two-fold symmetry superimposed with an anomalous Fourier map calculated from the SeMet data set with final phases contoured at 4σ . **b**, Section of the experimental electron-density map (contoured at 1σ) extended to 3.45 Å with the native data and superimposed with the refined NhaA model. Helix XII and the periplasmic helix XIp are connected by a well-defined loop. The short helices XIp (Phe 339) and IVc (Phe 136) are oriented in an anti-parallel manner with residue Asp 133 in an appropriate position for charge compensation.

¹Department of Molecular Membrane Biology, Max Planck Institute of Biophysics, Max-von-Laue-Str. 3, D-60438 Frankfurt, Germany. ²Alexander Silberman Institute of Life Sciences, Hebrew University of Jerusalem, Jerusalem 91904, Israel.

The structure was solved by single-wavelength anomalous dispersion (SAD) taking advantage of 10 SeMet positions per monomer. After solvent flattening and phase extension, the model was built and refined in iterative cycles to a final R_{work} of 29.6% and R_{free} of 31.7% to 3.45 Å resolution. The positions of the SeMet residues were important for model building and sequence assignment. Throughout model building and refinement the presence of a two-fold symmetry was used to constrain the atomic coordinates, and to improve refinement and electron-density map calculations. Experimental electron-density maps are shown in Fig. 1.

Overall architecture

NhaA consists of 388 amino-acid residues with the amino terminus and the carboxy terminus exposed to the cytoplasm²⁰. Our structural model comprises residues 9–384, which are arranged in 12 trans-membrane segments (TMSs; Fig. 2a), in line with previous results^{19,20}. The molecule measures about 40 Å × 45 Å, and its height is about 50 Å. The fold of NhaA is, to the best of our knowledge, previously undescribed; TMSs IV and XI (henceforth designated the TMSs IV/XI assembly) are of opposite orientations in the membrane and each is composed of a short helix, an extended polypeptide chain and a short helix (Fig. 2a, b). The short helices at the periplasmic and cytoplasmic sides are denoted p and c, respectively. In general, it is energetically unfavourable to insert a polar end of a helix in the low-dielectric core of the membrane. Moreover, helices IVc and XIp are oriented in an anti-parallel manner with their partially positive charged N termini facing each other in the middle of the membrane. The position of Asp 133 permits charge compensation and thus stabilization of the arrangement (Figs 1b and 2b). Together these two helices at lower resolution appear misleadingly like a single straight helix, which parallels helix V in close proximity (Fig. 2b). A similar anti-parallel architecture of two short helices with charge compensation exists in the chloride channel²¹. However, whereas in the latter the polypeptide chains turn back, the chains in NhaA cross each other, forming close contacts in the middle of the membrane, and each extends to a second short helix at the respective opposite side of the membrane (helices IVp and XIc, Fig. 2a, b). These latter helices are tilted with respect to helix V and their negative dipole ends are charge compensated by Lys 300 of helix X (Fig. 2b).

Other noteworthy elements are the S-shaped helices III and X, the bent helix IX and the extraordinarily short helices VII and VIII

(Fig. 2a). The membrane boundaries were estimated from the distribution of tryptophan and tyrosine residues²² (Fig. 2a). The periplasmic face of NhaA is flat and formed by structured loops close to the lipid bilayer. The longest loop, loop I–II, consists of a short helix (helix Ia, residues 35–41) followed by an anti-parallel, double-stranded β-sheet (β1, 45–48; β2, 55–58). It is oriented parallel to the membrane, providing a flat and rigid structure at the periplasmic boundary (Fig. 2a). At the cytoplasmic face more flexible loops, and several helices (II, V, IX and XII), protrude into the cytoplasm, creating a rough surface.

The TMSs are organized in two densely packed domains (A and B; Supplementary Fig. S1). Two bundles each containing three TMSs (III, IV and V; X, XI and XII) form domain A. Despite the weak sequence homology the two bundles are structurally related. It is a duplication with opposite orientation with respect to the membrane (Supplementary Fig. S2). Such structural repetitions have been observed in other membrane proteins^{21,23,24}. Domain B is formed by a linear bundle of six helices (II, VII, VIII, IX in the centre, I and VI peripherally attached at opposite sides). The two domains are in full agreement with the organization of helical bundles observed in the three-dimensional map of NhaA obtained by cryo-electron microscopy of two-dimensional crystals, which were also obtained at acidic pH (ref. 19).

At the centre of the domain interface a funnel opens to the cytoplasm (Fig. 3a, c, d, and Supplementary Fig. S1). It is formed by helices II and IX of domain B, helix IVc and its extended chain and helix V of domain A (Fig. 3a). The electrostatic potential surface viewed from the cytoplasm highlights strongly negatively charged patches lining the funnel (Fig. 3c, d). The rest of the cytoplasmic membrane surface is positively charged, whereas the periplasmic surface is negatively charged (Fig. 3e), in line with the positive-inside rule²⁵. The funnel is blocked approximately in the middle of the membrane at the crossing of the extended chains of the TMSs IV/XI assembly (Fig. 3a, d). A shallow negatively charged funnel opens to the periplasm and is formed by helices II, VIII and XIp (Fig. 3a, d, e). The cytoplasmic and periplasmic funnels point towards each other but do not form a continuous pore.

Structural basis for passage and binding site of substrates

This structure is a snapshot of the native, acidic pH-locked conformation of NhaA. Nevertheless, the cytoplasmic cation passage and a

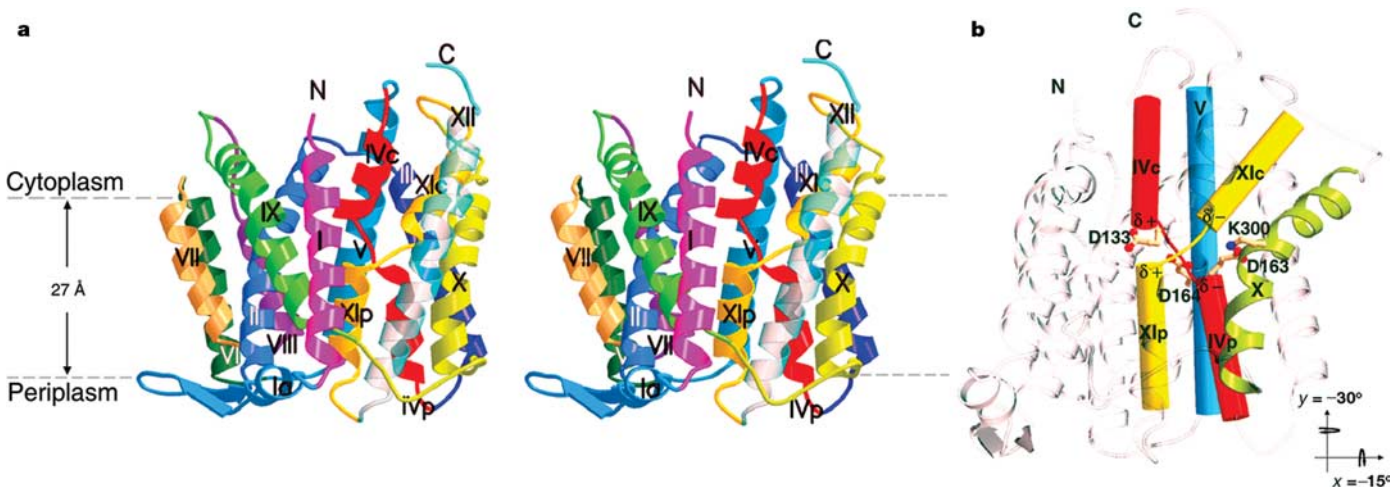


Figure 2 | Overall architecture of NhaA. **a**, Stereo view of a ribbon representation viewed parallel to the membrane (grey broken lines). The 12 TMSs are labelled with roman numerals; they comprise the following residues: 12–30 (I), 59–85 (II), 95–116 (III), 121–131 (IVp), 134–143 (IVc), 150–175 (V), 182–200 (VI), 205–218 (VII), 223–236 (VIII), 247–271 (IX), 290–311 (X), 327–336 (XIc), 340–350 (XIp) and 357–382 (XII). N and C

indicate the N and C termini. **b**, TMSs IV/XI assembly. Helices of the assembly and helix V are shown as cylinders, helix X in ribbon representation. The partial charges of the N and C termini of the short helices are indicated. The orientation of the molecule is indicated with respect to **a**.

most probable binding site for Na^+ and Li^+ , the specific substrates of NhaA, are clearly evident in the structure. The negatively charged funnel is very well suited to attract cations and to increase their local concentrations over that of anions (Fig. 3a). A cluster of three negatively charged residues, Glu 78, Glu 82 and Glu 252, is located on one side of the funnel entrance and residue Asp 11 is on the opposite side (Fig. 3a). An accessibility analysis of the cavity for ions and water with the use of the respective ion radii as the probe size (3.58, 3.82 and 3.31 Å for hydrated Na^+ , Li^+ and K^+ , respectively; 0.95 and 0.6 Å for non-hydrated Na^+ and Li^+ , respectively, and 1.4 Å for water) was performed. The funnel is not selective for cations above the level of the four acidic residues (Glu 78, Glu 82, Glu 252 and Asp 11), and hydrated Na^+ , Li^+ and K^+ as well as water can diffuse into it (Fig. 3a). Subsequently, the passage narrows and is lined by nonpolar residues. Fully hydrated Na^+ or Li^+ ions cannot access the end of the funnel in the middle of the membrane, where Asp 164 of helix V is positioned (Fig. 3a). Although non-hydrated substrates could in principle reach this acidic residue, the structure does not provide a clue as to whether dehydration of the cations occurs in this conformation of NhaA.

The specific location of Asp 164 strongly suggests that it contributes to the Na^+/Li^+ -binding site (Fig. 3a, b, d). Structures of Na^+ -binding proteins demonstrate that the smallest alkali-metal ions are ligated by oxygen atoms provided by water as well as main-chain carbonyl, carboxyl or hydroxyl groups with an average coordination number of five to six (refs 26, 27). Further residues are therefore expected to contribute to the putative Na^+/Li^+ -binding site of NhaA. Indeed, additional polar and/or ionizable amino-acid residues are located near Asp 164 in the centre of the TMSs assembly IV/XI, namely Asp 163 of helix V, and Asp 133 and Thr 132 of TMS IV; they are excluded from the ion passage (Figs 3a, b and 4). Biochemical and

genetic data obtained with NhaA activated at alkaline pH provide a strong clue to the role of these residues in the active conformation. Both Asp 164 and Asp 163 are highly conserved residues and are essential, which is in line with their proposed role in ion binding²⁸. Residues Asp 133 and Thr 132 are also highly conserved but are not essential. However, a mutational change in the two latter residues markedly increased the apparent K_m of the antiporter to both Na^+ and Li^+ , indicating their possible structural role and/or involvement in the translocation mechanism²⁹. It should be noted that Na^+ is not observed in the structure. This might be due to the medium resolution and/or to the partly exposed binding site seen in the acidic-pH-locked conformation of NhaA.

At the periplasmic side, Asp 65 of helix II is located at the tip of the shallow funnel, 16 Å away from Asp 164 (Fig. 3a, d). This funnel is separated from the putative Na^+/Li^+ -binding site by densely packed non-polar residues of helices II, IVp and XIp, which are not accessible to either water or ions, thus forming the periplasmic barrier (Fig. 3a). Hence, the most evident features of the acidic pH-locked structure are the following: first, the cytoplasmic ion passage ending with a narrow cavity that does not allow fully hydrated Na^+ and Li^+ to access the binding site; second, the putative binding site in the centre of the membrane, of which only Asp 164 is exposed to the cytoplasmic ion passage; and last, the barrier at the periplasmic side, to which the TMSs IV/XI assembly contributes.

Mechanism of the pH-regulated Na^+/H^+ exchange

The main physiological role of NhaA is the regulation of cytoplasmic pH and Na^+ (Li^+) content. To maintain a constant intracellular pH of about 7.6 at more alkaline extracellular pH, surplus Na^+ (Li^+), which is toxic to the cell, is excreted in exchange for protons¹². NhaA is tightly regulated by pH. Its activity alters for more than three orders

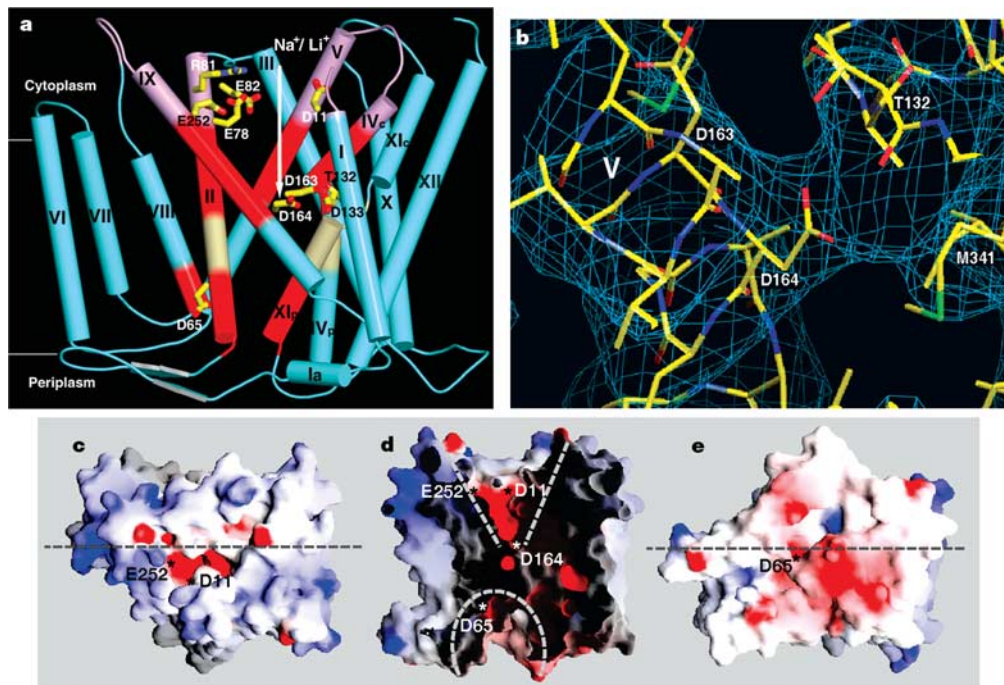


Figure 3 | Substrate passage and periplasmic barrier. **a**, The TMSs lining the cytoplasmic and the periplasmic cation passage are highlighted by colours in the cylinder representation. The cavities were analysed for ion and water accessibility by using the programs CastP and Voidoo^{49,50}. Fully hydrated Na^+/Li^+ can diffuse into the upper zone of the cytoplasmic funnel (light purple) but can enter neither the lower part of it (red) nor the periplasmic funnel (red). The barrier between the passages is coloured in cream. **b**, The putative catalytic site of NhaA viewed from the cytoplasm along the membrane normal. The electron-density map ($2F_o - F_c$

contoured at 1σ) superimposed with the refined model is shown. **c–e**, The electrostatic potential surface coloured according to its charge (positive in blue, negative in red). Some residue positions (asterisks) are indicated for orientation. **c**, Cytoplasmic view along the membrane normal. **d**, Cross-section through the antiporter with the front part removed along the membrane normal. The position of the section is indicated in **c** and **e** (horizontal line). Cytoplasmic (top) and periplasmic (bottom) funnels are marked by broken lines. **e**, Periplasmic view along the membrane normal.

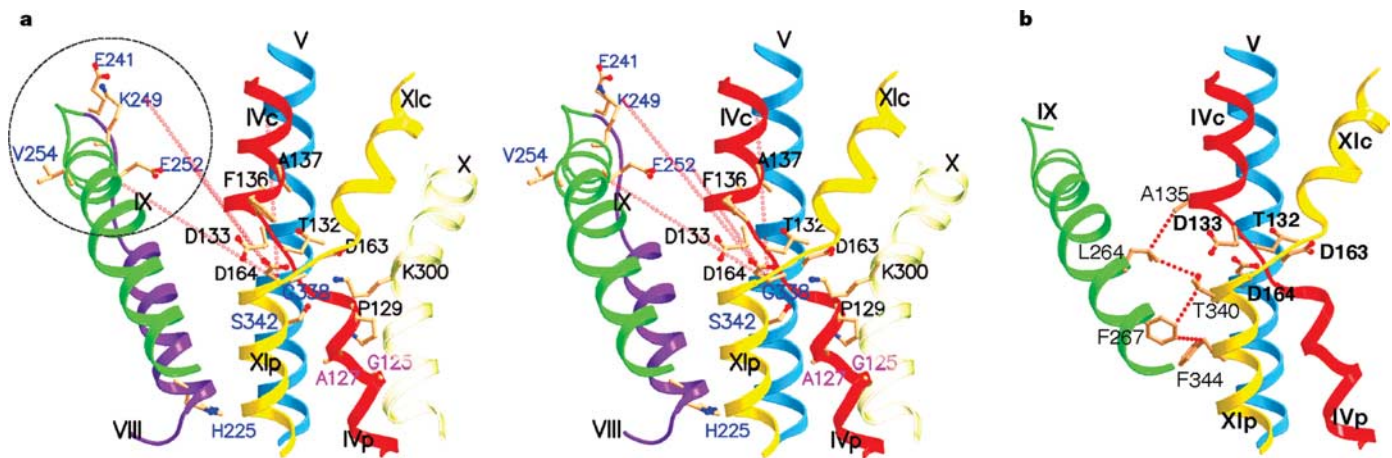


Figure 4 | Structural basis of Na^+/H^+ translocation and pH regulation. **a**, Stereo view of TMSs oriented parallel to the membrane, with the cytoplasmic side at the top. The colour code is as in Fig. 2. Residues whose alterations affect pH regulation^{12,16,31}, apparent K_m (refs 29, 38) or both^{29,38} are shown with side chains and labelled blue, black and purple, respectively.

The putative 'pH sensor' is encircled. The approximate position of the cytoplasmic passage is marked by red dotted lines connecting Asp 164 with residues lining the funnel entry. **b**, Close interactions between helix IX and helices IVc and XIp that are important for pH regulation. Van der Waals contacts between side chains are indicated with dotted red lines.

of magnitude between pH 7 and 8 and it is fully downregulated below pH 6.5 (refs 12, 13). Several questions can be raised about the structure of the acidic pH-locked NhaA. Where is the 'pH sensor'? What is the structural element that transmits and converts the pH signal into a change in activity? How is the change accomplished? The structure reveals that the NhaA N terminus and residue Glu 252 of helix IX at the cytoplasmic funnel entrance are adjacent (Figs 2a and 3a), in line with previous crosslinking data^{30,31}. Mutagenesis of amino-acid residues clustered in these locations and loop VIII–IX drastically affects the pH dependence of NhaA^{16,31,32} (Fig. 4a). Furthermore, conformational changes induced by alkaline pH occur in these locations as probed by accessibility tests: at the N terminus with a monoclonal antibody³², at the N terminus of helix IX with trypsin¹⁶ (Lys 249; Fig. 4a) or with a fluorescent probe³¹ (E252C; Fig. 4a). Most importantly, the pH dependence of these conformational changes at the cytoplasmic side parallels the pH dependence of NhaA activation¹². We therefore suggest that a 'pH sensor', in which a pH signal results in alteration of the protonation state, is located at the entrance of the cytoplasmic passage (Fig. 4a) and that it elicits conformational changes that are transmitted to activate NhaA. In agreement with this, the pH signal is perceived in cells from the cytoplasm³³.

Helix IX is the most likely structural element capable of transmitting the pH signal required to activate NhaA (Fig. 4). It is distorted, a feature that allows flexibility for a long-range conformational change. Its N terminus contributes to the 'pH sensor' and it itself undergoes a pH-induced conformational change^{16,31}. Close to its kink at the centre of the membrane it is in direct contact with the TMSs IV/XI assembly (Fig. 4b), an essential part of the Na^+/H^+ exchange machinery (see below).

The generally accepted model explaining Na^+/H^+ exchange³⁴ and many other secondary transport processes^{35,36} is the alternating-access mechanism. In this model, the transporter has two major alternating conformations with the substrate-binding site facing either inwards or outwards. Interconversion between the two conformations in an antiporter is only possible through a substrate-bound form of the protein. For NhaA that means that either one Na^+/Li^+ or two H^+ are bound³⁷. The two aspartates of the binding site are located on the straight helix V, which does not have conspicuous structural features for conformational changes. In contrast, the TMSs IV/XI assembly, with its short helices and their dipoles compensated for in the middle of the membrane by Asp 133 and Lys 300, is most suitable for charge-induced subtle and fast

conformational changes. On the basis of these unique structural features we suggest that a pH-regulated movement of the extended chains of the TMSs IV/XI assembly allows alternating access of the substrate-binding site to either the intracellular or extracellular space (Fig. 5).

At acidic pH, when it is downregulated, only part of the cation-binding site (Asp 164) is exposed to the cation passage while the periplasmic passage is blocked by the ion-barrier formed partly by helix XIp (Figs 3a and 5a). We suggest that at alkaline pH, in response to a signal from the 'pH sensor', a conformational change of helix IX results in the reorientation of helices XIp and IVc. This would expose the full Na^+/Li^+ -binding site (Asp 164, Asp 163 and most probably Thr 132) to the cytoplasmic passage and remove the periplasmic ion barrier, leaving the extended chain to seal the binding site from the periplasm (Fig. 5b). This conformation would now be ready for Na^+/H^+ exchange. Binding of Na^+/Li^+ to the active site from the cytoplasm would result in a charge imbalance that then would trigger a small movement of XIp and IVc and their extended chains. The cation-loaded binding site would thus then be exposed to the periplasm and sealed from the cytoplasm (Fig. 5c). On release of Na^+/Li^+ , both aspartates would become protonated, thereby inducing a conformational change that would expose them back to the cytoplasm; deprotonation would complete the cycle (Fig. 5b). This model permits an overall stoichiometry of one Na^+/Li^+ exported in exchange for two protons taken up. Because NhaA is reversible, the magnitude of the electrochemical potential difference of Na^+/Li^+ compared with that of H^+ determines the direction of the cation exchange across the membrane. The rate of exchange would be determined by the rate of movement of the extended chains and helices IVc and XIp in response to pH. Acidic pH locks NhaA, whereas alkaline pH activates it (Fig. 5a).

This working model is strongly supported by genetic and biochemical data obtained at alkaline pH, at which NhaA is active. The measured $\text{Na}^+:\text{H}^+$ stoichiometry³⁷ of the exchange is 1:2. Many residues in TMS IV are conserved in the NhaA protein family, and their mutations markedly affect³⁸ the apparent K_m for Na^+ and Li^+ (Fig. 4a). Furthermore, the need for the reorientation of helix IVc with respect to XIp is strongly supported by the double mutant F136C/S342C (ref. 38). This mutant forms a disulphide bond that inhibits transport, and reducing the bond restores activity in a reversible manner³⁸. Extensive crosslinking data are in accordance with the close contacts between the TMSs of the assembly³⁸ and their crucial role for activity and pH regulation^{29,38}. The most informative

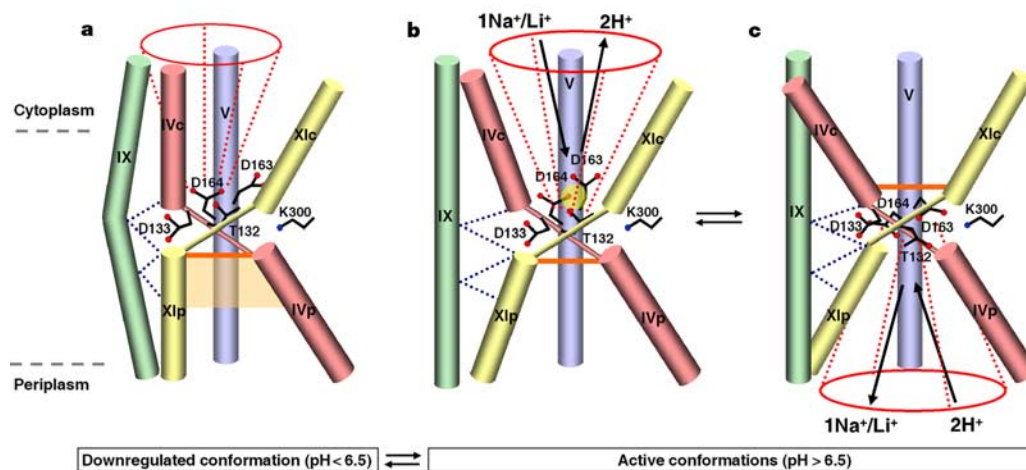


Figure 5 | Proposed mechanism of pH regulation and translocation of NhaA. The TMSs IV/XI assembly, the charge-compensating residues Asp 133 and Lys 300, and further structural elements involved are shown schematically. **a**, Acidic pH-locked conformation. Ion transport is prevented by the periplasmic ion barrier (transparent, cream-coloured area) and by the only partly exposed $\text{Na}^+(\text{Li}^+)$ -binding site (residues Asp 164, Asp 163 and Thr 132). **b**, Activation by alkaline pH induces conformational changes in helix IX resulting in the reorientation of helices IVc and XIp (interactions

indicated by blue dotted lines). The putative $\text{Na}^+(\text{Li}^+)$ -binding site (yellow transparent circle) is now exposed to the cytoplasmic funnel (red dotted lines and red circle) and sealed towards the periplasm (orange bar). **c**, $\text{Na}^+(\text{Li}^+)$ binding results in the opening of the periplasmic funnel and the exposure of the active site to the periplasm. The cation is released. Protonation of the aspartates (Asp 164 and Asp 163) brings the antiporter back to the active conformation open to the cytoplasm.

examples are the mutants G338S (ref. 39) and G338C (ref. 38) of the extended chain XI (Fig. 4a) that completely remove the pH control and produce NhaA variants that are fully active independently of pH. In the inactive double variant T132C/G338C both activity and pH control can be partly restored by re-establishing the physical interaction between the extended chains by chemical crosslinking³⁸.

Discussion

The physical separation between the 'pH sensor' and the exchange machinery revealed by the structure entails long-range, pH-induced conformational changes for pH activation. This observation is in agreement with biochemical data obtained from both prokaryotic¹² and eukaryotic Na^+/H^+ antiporters^{40,41}. The suggested mechanism of Na^+/H^+ exchange of the alkaline pH-activated NhaA is based on small conformational changes limited to a small part of the protein. In contrast, the structures of four secondary transporters^{42–45} have recently indicated a different structural basis for the transport mechanism. Heavily distorted helices with kinks and bends lining a wide substrate passage provide structural flexibility, thereby allowing the molecule to assume different conformations. This type of mechanism is suitable for these slow transporters of large organic molecules with catalytic-centre activities (turnover numbers) of 600, 800 and $1,440 \text{ min}^{-1}$ (LacY (ref. 46), ADP/ATP antiporter⁴⁷ and GlpT antiporter⁴⁸, respectively). In contrast, NhaA is one of the fastest transporters known¹³, with a catalytic-centre activity of $89,000 \text{ min}^{-1}$. The suggested mechanism of Na^+/H^+ exchange, based on subtle conformational changes in the centre of the molecule, is therefore most suitable for the very high activity of NhaA.

Although many aspects of the ion-translocation mechanism and pH regulation are illuminated by this NhaA structure, higher-resolution structural determinations with Li^+ or Na^+ bound are required to understand the ligand binding and translocation mechanism at the atomic level. The alkaline pH-induced conformation is essential for a further understanding of the pH control and proton access to the binding site.

METHODS

Overexpression and purification. Cells of *E. coli* RK20 were co-transformed with the plasmids pAXH and pI^Q encoding His-tagged NhaA and LacI^Q,

respectively. The gene *nhaA*, which was deleted from strain RK20, was expressed from the plasmid after induction with isopropyl- β -D-thiogalactoside. Membranes were prepared from broken cells by differential centrifugation. The protein was solubilized in 1% n-dodecyl- β -D-maltopyranoside solution and purified on a nickel-affinity column. The detergent was exchanged on the column with 0.03% n-dodecyl- α -D-maltopyranoside. The eluted protein was concentrated and supplemented with 20% w/v sucrose. SeMet-labelled protein was produced and purified accordingly, but with *E. coli* B834DE3 (Novagen) cells were grown in minimal medium containing seleno-L-methionine.

Crystallization. Crystals were grown at 6 °C by hanging-drop vapour diffusion by mixing equal volumes of protein ($4\text{--}6 \text{ mg ml}^{-1}$) and reservoir solution (28–34% v/v poly(ethylene glycol) 400, 200–450 mM MgCl_2 , 100 mM KCl, 25 mM sodium citrate pH 4, 1% n-octyl- β -D-glucopyranoside and 0.5% ethanol). Crystals were flash-cooled to 100 K with nitrogen.

Structure determination and refinement. Diffraction data were collected at the ESRF beam lines ID29 (data set SeMet SAD, 4.3 Å resolution) and ID23 (data set Native 1, 3.8 Å resolution) and at the SLS beam line PX06 (data set Native 2, 3.45 Å resolution) with charge-coupled device detectors and cryo-cooling at 100 K (Supplementary Table S1). The structure was solved by SAD, locating 20 selenium atoms. Phases were calculated to 4.3 Å ($17\text{Å--}4.3\text{Å}$) with a figure of merit of 0.42 for acentric reflections and 0.13 for centric reflections. The SAD phases were applied to the native data set (Native 1) and gradually extended to 3.8 Å with solvent flattening, histogram matching and averaging options. Model building and refinement were facilitated by locating the selenium atom positions in anomalous difference maps from the SeMet data (Fig. 1a) and by keeping a tight two-fold non-crystallographic symmetry restraint during refinement. For final refinement of the model the second native data set at 3.45 Å was used.

Further information. Detailed information on methodological aspects is provided as Supplementary Information.

Received 20 October 2004; accepted 22 April 2005.

- West, I. & Mitchell, P. Proton/sodium ion antiport in *Escherichia coli*. *Biochem. J.* **144**, 87–90 (1974).
- Padan, E., Venturi, M., Gerchman, Y. & Dover, N. Na^+/H^+ antiporters. *Biochim. Biophys. Acta* **1505**, 144–157 (2001).
- Orlowski, J. & Grinstein, S. Diversity of the mammalian sodium/proton exchanger SLC9 gene family. *Pflugers Arch.* **447**, 549–565 (2004).
- Counillon, L. & Pouyssegur, J. The expanding family of eucaryotic Na^+/H^+ exchangers. *J. Biol. Chem.* **275**, 1–4 (2000).
- Engelhardt, S., Hein, L., Keller, U., Klambt, K. & Lohse, M. J. Inhibition of Na^+/H^+ exchange prevents hypertrophy, fibrosis, and heart failure in β 1-adrenergic receptor transgenic mice. *Circ. Res.* **90**, 814–819 (2002).
- Myers, M. L. in *The Sodium-Hydrogen Exchange, from Molecule to its Role in Disease* (eds Karmazyn, N., Avkiran, M. & Fliegel, L.) 279–290 (Kluwer Academic, Boston, Massachusetts, 2003).

7. Apse, M. P., Sottosanto, J. B. & Blumwald, E. Vacuolar cation/H⁺ exchange, ion homeostasis, and leaf development are altered in a T-DNA insertional mutant of AtNHX1, the *Arabidopsis* vacuolar Na⁺/H⁺ antiporter. *Plant J.* **36**, 229–239 (2003).
8. Qiu, Q. S., Barkla, B. J., Vera-Estrella, R., Zhu, J. K. & Schumaker, K. S. Na⁺/H⁺ exchange activity in the plasma membrane of *Arabidopsis*. *Plant Physiol.* **132**, 1041–1052 (2003).
9. Apse, M. P., Aharon, G. S., Snedden, W. A. & Blumwald, E. Salt tolerance conferred by overexpression of a vacuolar Na⁺/H⁺ antiport in *Arabidopsis*. *Science* **285**, 1256–1258 (1999).
10. Krulwich, T. A., Ito, M. & Guffanti, A. A. The Na⁺-dependence of alkaliphily in *Bacillus*. *Biochim. Biophys. Acta* **1505**, 158–168 (2001).
11. Hase, C. C. & Mekalanos, J. J. Effects of changes in membrane sodium flux on virulence gene expression in *Vibrio cholerae*. *Proc. Natl Acad. Sci. USA* **96**, 3183–3187 (1999).
12. Padan, E., Tzuberly, T., Herz, K., Kozachkov, L. & Galili, L. NhaA of *Escherichia coli*, as a model of a pH regulated Na⁺/H⁺ antiporter. *Biochim. Biophys. Acta* **1658**, 2–13 (2004).
13. Taglicht, D., Padan, E. & Schuldiner, S. Overproduction and purification of a functional Na⁺/H⁺ antiporter coded by *nhaA* (ant) from *Escherichia coli*. *J. Biol. Chem.* **266**, 11289–11294 (1991).
14. Putney, L. K., Denker, S. P. & Barber, D. L. The changing face of the Na⁺/H⁺ exchanger, NHE1: structure, regulation and cellular actions. *Annu. Rev. Pharmacol. Toxicol.* **42**, 527–552 (2002).
15. Wakabayashi, S., Pang, T., Hisamitsu, T. & Shigekawa, M. in *The Sodium–Hydrogen Exchange, from Molecule to its Role in Disease* (eds Karmazyn, N., Avkiran, M. & Fliegel, L.) 35–49 (Kluwer Academic, Boston, Massachusetts, 2003).
16. Gerchman, Y., Rimon, A. & Padan, E. A pH-dependent conformational change of NhaA Na⁺/H⁺ antiporter of *Escherichia coli* involves loop VIII–IX, plays a role in the pH response of the protein, and is maintained by the pure protein in dodecyl maltoside. *J. Biol. Chem.* **274**, 24617–24624 (1999).
17. Gerchman, Y., Rimon, A., Venturi, M. & Padan, E. Oligomerization of NhaA, the Na⁺/H⁺ antiporter of *Escherichia coli* in the membrane and its functional and structural consequences. *Biochemistry* **40**, 3403–3412 (2001).
18. Williams, K. A., Geldmacher-Kaufner, U., Padan, E., Schuldiner, S. & Kuhlbrandt, W. Projection structure of NhaA, a secondary transporter from *Escherichia coli*, at 4.0 Å resolution. *EMBO J.* **18**, 3558–3563 (1999).
19. Williams, K. A. Three-dimensional structure of the ion-coupled transport protein NhaA. *Nature* **403**, 112–115 (2000).
20. Rothman, A., Padan, E. & Schuldiner, S. Topological analysis of NhaA, a Na⁺/H⁺ antiporter from *Escherichia coli*. *J. Biol. Chem.* **271**, 32288–32292 (1996).
21. Dutzler, R., Campbell, E. B., Cadene, M., Chait, B. T. & MacKinnon, R. X-ray structure of a ClC chloride channel at 3.0 Å reveals the molecular basis of anion selectivity. *Nature* **415**, 287–294 (2002).
22. Palsdottir, H. & Hunte, C. Lipids in membrane protein structures. *Biochim. Biophys. Acta* **1666**, 2–18 (2004).
23. Fu, D. *et al.* Structure of a glycerol-conducting channel and the basis for its selectivity. *Science* **290**, 481–486 (2000).
24. Khademi, S. *et al.* Mechanism of ammonia transport by Amt/MEP/Rh: structure of AmtB at 1.35 Å. *Science* **305**, 1587–1594 (2004).
25. von Heijne, G. Membrane protein structure prediction: hydrophobicity analysis and the 'positive inside' rule. *J. Mol. Biol.* **225**, 487–494 (1992).
26. Glusker, J. P. Structural aspects of metal liganding to functional groups in proteins. *Adv. Protein Chem.* **42**, 1–76 (1991).
27. Harding, M. M. The architecture of metal coordination groups in proteins. *Acta Crystallogr. D Biol. Crystallogr.* **60**, 849–859 (2004).
28. Inoue, H., Noumi, T., Tsuchiya, T. & Kanazawa, H. Essential aspartic acid residues, Asp-133, Asp-163 and Asp-164, in the transmembrane helices of a Na⁺/H⁺ antiporter (NhaA) from *Escherichia coli*. *FEBS Lett.* **363**, 264–268 (1995).
29. Galili, L., Rothman, A., Kozachkov, L., Rimon, A. & Padan, E. Trans membrane domain IV is involved in ion transport activity and pH regulation of the NhaA-Na⁺/H⁺ antiporter of *Escherichia coli*. *Biochemistry* **41**, 609–617 (2002).
30. Rimon, A., Tzuberly, T., Galili, L. & Padan, E. Proximity of cytoplasmic and periplasmic loops in NhaA Na⁺/H⁺ antiporter of *Escherichia coli* as determined by site-directed thiol cross-linking. *Biochemistry* **41**, 14897–14905 (2002).
31. Tzuberly, T., Rimon, A. & Padan, E. Mutation E252C increases drastically the *K_m* for Na and causes an alkaline shift of the pH dependence of NhaA Na⁺/H⁺ antiporter of *Escherichia coli*. *J. Biol. Chem.* **279**, 3265–3272 (2004).
32. Venturi, M. *et al.* The monoclonal antibody 1F6 identifies a pH-dependent conformational change in the hydrophilic NH₂ terminus of NhaA Na⁺/H⁺ antiporter of *Escherichia coli*. *J. Biol. Chem.* **275**, 4734–4742 (2000).
33. Zilberstein, D., Agmon, V., Schuldiner, S. & Padan, E. The sodium/proton antiporter is part of the pH homeostasis mechanism in *Escherichia coli*. *J. Biol. Chem.* **257**, 3687–3691 (1982).
34. Jin, J., Guffanti, A. A., Bechhofer, D. H. & Krulwich, T. A. Tet(L) and tet(K) tetracycline-divalent metal/H⁺ antiporters: characterization of multiple catalytic modes and a mutagenesis approach to differences in their efflux substrate and coupling ion preferences. *J. Bacteriol.* **184**, 4722–4732 (2002).
35. Jencks, W. P. The utilization of binding energy in coupled vectorial processes. *Adv. Enzymol.* **51**, 75–106 (1980).
36. West, I. C. Ligand conduction and the gated-pore mechanism of transmembrane transport. *Biochim. Biophys. Acta* **1331**, 213–234 (1997).
37. Taglicht, D., Padan, E. & Schuldiner, S. Proton–sodium stoichiometry of NhaA, an electrogenic antiporter from *Escherichia coli*. *J. Biol. Chem.* **268**, 5382–5387 (1993).
38. Galili, L., Hertz, K., Dym, O. & Padan, E. Unraveling functional and structural interactions between trans membrane domains IV and XI of NhaA Na⁺/H⁺ antiporter of *Escherichia coli*. *J. Biol. Chem.* **279**, 23104–23113 (2004).
39. Rimon, A., Gerchman, Y., Kariv, Z. & Padan, E. A point mutation (G338S) and its suppressor mutations affect both the pH response of the NhaA-Na⁺/H⁺ antiporter as well as the growth phenotype of *Escherichia coli*. *J. Biol. Chem.* **273**, 26470–26476 (1998).
40. Aronson, P. Kinetic properties of the plasma membrane Na⁺/H⁺ exchanger. *Annu. Rev. Physiol.* **47**, 545–560 (1985).
41. Wakabayashi, S., Hisamitsu, T., Pang, T. & Shigekawa, M. Kinetic dissection of two distinct proton binding sites in Na⁺/H⁺ exchangers by measurement of reverse mode reaction. *J. Biol. Chem.* **278**, 43580–43585 (2003).
42. Murakami, S., Nakashima, R., Yamashita, E. & Yamaguchi, A. Crystal structure of bacterial multidrug efflux transporter AcrB. *Nature* **419**, 587–593 (2002).
43. Abramson, J. *et al.* Structure and mechanism of the lactose permease of *Escherichia coli*. *Science* **301**, 610–615 (2003).
44. Pebay-Peyroula, E. *et al.* Structure of mitochondrial ADP/ATP carrier in complex with carboxyatractyloside. *Nature* **426**, 39–44 (2003).
45. Huang, Y., Lemieux, M. J., Song, J., Auer, M. & Wang, D. N. Structure and mechanism of the glycerol-3-phosphate transporter from *Escherichia coli*. *Science* **301**, 616–620 (2003).
46. Viitanen, P., Garcia, M. L. & Kaback, H. R. Purified reconstituted lac carrier protein from *Escherichia coli* is fully functional. *Proc. Natl Acad. Sci. USA* **81**, 1629–1633 (1984).
47. Klingenberg, M. in *The ADP/ATP Carrier in Mitochondrial Membranes* (ed. Martonosi, A. N.) (Plenum, New York, 1985).
48. Auer, M. *et al.* High-yield expression and functional analysis of *Escherichia coli* glycerol-3-phosphate transporter. *Biochemistry* **40**, 6628–6635 (2001).
49. Liang, J., Edelsbrunner, H. & Woodward, C. Anatomy of protein pockets and cavities: measurement of binding site geometry and implications for ligand design. *Protein Sci.* **7**, 1884–1897 (1998).
50. Kleywegt, G. J. & Jones, T. A. Detection, delineation, measurement and display of cavities in macromolecular structures. *Acta Crystallogr. D Biol. Crystallogr.* **50**, 178–185 (1994).

Supplementary Information is linked to the online version of the paper at www.nature.com/nature.

Acknowledgements We acknowledge the beamtime and the assistance of the personnel at beamlines ID29 and ID23 at the European Synchrotron Facility and at PX06 at the Swiss Light Source. This study was supported by grants from the German Israeli Foundation for Scientific Research and Development (to H.M. and E.P.), the Max Planck Society, the Fonds der Chemischen Industrie and the Israel Science Foundation (to E.P.). E.S. was supported by the International Max Planck Research School (IMPRS).

Author Information Coordinates have been deposited in the Protein Data Bank under accession code 1ZCD. Reprints and permissions information is available at npg.nature.com/reprintsandpermissions. The authors declare no competing financial interests. Correspondence and requests for materials should be addressed to C.H. (carola.hunte@mpibp-frankfurt.mpg.de), E.P. (etana@vms.huji.ac.il) or H.M. (hartmut.michel@mpibp-frankfurt.mpg.de).